A New Design of a Submicropositioner Utilizing Electromagnetic Actuators and Flexure Mechanism

Mei-Yung Chen, Hsuan-Han Huang, and Shao-Kang Hung, *Member, IEEE*

***Abstract*—In this paper, a novel XY-dimensional submicropositioner, including mechanism, control, and analysis, is successfully presented. The design of the submicropositioner utilizes a monolithic parallel flexure mechanism with built-in electromagnetic actuators and optical sensors to achieve the object of 3-DOF precise motion. From the provided experimental results, there are several main goals that have been achieved in this paper: 1) to integrate the electromagnetic actuator and the parallel flexure mechanism for planar positioning system; 2) to establish the mathematical modeling; 3) to develop an advanced adaptive sliding-mode controller; and 4) to perform extensive experiments to test the realistic performance.**

***Index Terms*—Adaptive controller, electromagnetic actuator, Fabry–Perot interferometer, modeling, motion control, optical sensor, parallel flexure mechanism, precision positioner, sliding mode controller (SMC).**

NOMENCLATURE

B_i, $i = 1, 2, 3, 4$	Magnetic flux density through each conducting wire.
i_i, $i = 1, 2, 3, 4$	Current carried on the conducting wires.
d_i, $i = 1, 2, 3, 4$	Distances from the center of the platen to the center of the actuators.
f_{di}, $i = 1, 2, 3, 4$	Elastic forces.
f_{x1}, f_{x2}, f_{y3}, f_{y4}	Force actuated by the nth actuator in X-axis or Y-axis.
x_1, x_2, y_3, y_4	Displacements of each magnet.
L	Edge length of the coil.
f_{act}	Actuated force.
K_I	Current–force constant.
$w^d = [f_X^d \ f_Y^d \ \tau^d]^{\text{T}}$	Total forces and torque on the platen.
$f_{\max}$	Actuator maximum force.
M, I	Mass and inertia of the platen.
b_x, b_y, b_θ	Damping constants.
k_x, k_y	Modulus of elasticity.

Manuscript received February 13, 2009; revised September 14, 2009. First published October 6, 2009; current version published December 11, 2009. This work was supported by the National Science Council, R.O.C., under Grant NSC-95-2516-S-003-019-MY3.

M.-Y. Chen is with the Department of Mechatronic Technology, National Taiwan Normal University, Taipei 10610, Taiwan (e-mail: cmy@ntnu.edu.tw).

H.-H. Huang was with National Taiwan University, Taipei 106, Taiwan. He is now with MediaTek Inc., Hsinchu 300, Taiwan (e-mail: han.huang@mediatek.com).

S.-K. Hung is with the Department of Mechanical Engineering, National Chiao Tung University, Hsinchu 300, Taiwan (e-mail: skhung@mail.nctu.edu.tw).

Digital Object Identifier 10.1109/TIE.2009.2033091

I. INTRODUCTION

HIGH-PRECISION positioning technology is essential in various advanced applications. One whole positioning system consists of a moving platform, an actuating system, and a measuring system as feedback. In each part, there are many kinds of solutions to implement. In macro application, a common method of positioning is through the use of the leadscrew [1]–[4]. Despite the features of high stiffness, thrust, and speed, leadscrews suffer from lost motion, stick slip, and windup. The dry friction has been neglected in macro motion, but it is one of the most important factors limiting the performance in the precision positioning application. Therefore, to prevent the problem of such dry friction and backlash, regardless of the size of the traveling range, there are four common types of mechanisms used: inchwormlike-clamping, inertial sliding/walking, flexure, and levitated mechanisms. In the inchwormlike-clamping mechanism, numerous designs of inchworm motors have been suggested in [5]. Piezoelectric inchworm precision positioners are also widely discussed in [6]. For the sliding/walking mechanism, the multiaxis positioning device has been developed [7]. The third type of mechanisms uses suspension to levitate the moving platform. Due to its noncontact characteristics, it is also commonly used to prevent dry friction. Air-levitated [8] and magnetic-levitated [9], [10] mechanisms have been proposed. The fourth type of mechanisms is based on the elastic deformation of material, the so-called flexure hinge mechanism. Precision mechanisms use flexures as replacement for conventional hinges to prevent problems with friction. Furthermore, in some cases, long-range single-degree-of-freedom flexure stages have been designed [11]–[15], but large-range XY-flexure stages are relatively scarce in the current technical literature.

In the precision positioning field, most of the current high-precision positioning devices utilize piezoelectric materials for actuation. The crystal lattices of the piezoelectric material deform when subjected to an electric field. Several advantages of these actuators are repeatable submicrometer motion, no backlash, no wear and tear suffered, fast response time, etc. [16]–[18]. Commercial products, such as miniature piezopositioners and scanners [19], are manufactured by *Physik Instrumente*. However, its scan range is only 80 μm. The main disadvantage of a piezoelectric actuator is shorter travel range. There is generally a tradeoff between high-resolution positioning and larger range positioning. To enlarge the travel range, the electromagnetic actuation has been currently applied in the precision field [20]–[22]. In particular, the magnetic actuator technique with no mechanical contact is typically adopted in high-precision machinery [23]–[30]. Based on this technique,

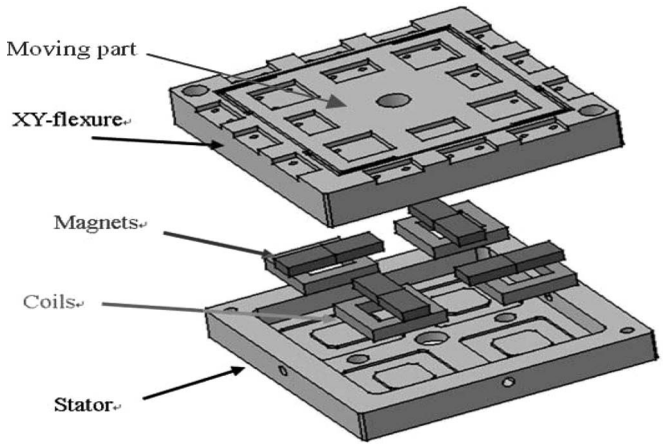

Fig. 1. Exploded view of the positioner.

some XY stages [31], [32] were designed by dual-axis structures. The most serious ones are the lack of sufficient robustness and excessive power consumption. In order to eliminate these problems and to design a precision positioner with larger travel range to improve the commercial feasibility of the emerging technologies, a novel 3-DOF positioning system using the single-layer structure will be presented in this paper.

Above all, a compact precision positioning (submicrometer-level) and larger travel range (millimeter-level) positioner is the goal of this paper. This paper concerns the integration of the parallel flexure mechanism and electromagnetic drives with optical sensors serving as feedback sensors to achieve a high-precision positioner. Moreover, the stabilizing controller to be developed should be robust enough to tolerate these inevitable uncertainties and unmodeled dynamics. One of the methodology fields is named as adaptive sliding-mode controller (ASMC), which can perform online system identification implicitly or explicitly while tuning the controller gains to guarantee the stability of the closed-loop system [33]–[37].

II. System Description and Modeling of the Submicropositioner

The positioner, shown in an exploded view in Fig. 1, includes the stator, XY-flexure stage, and four sets of electromagnetic actuators. Each actuator is assembled by one coil and two permanent magnets. The magnets of the actuator are mounted on the moving part of the XY flexure, and the coils are mounted on the stator. The air gap between the magnet and the coil is 50 μm. By this way of mounting, we can make the moving part wireless and prevent the friction generated when it moves.

The principle of the actuator is based on the voice coil motor (VCM) [38]–[40]. One set of actuators can generate a linear motion in one dimension. The detailed working principle of the VCM will be described in Section II-A. The guiding mechanism of the XY flexure is shown in Fig. 2. By installing four sets of these actuators orthogonal to each other, we can achieve both translation along the X- and Y-axes and rotation around the θ-axis of the moving part. In this paper, we choose a fiber Fabry–Perot interferometer as the measurement sensor due to its low cost [41]. The maximum translations in the X- and Y-axes are $\pm$0.5 mm, and the maximum rotation in θ-axis is 5°, which is constrained by the XY-flexure mechanism configurations and the effective measurement range of the sensors.

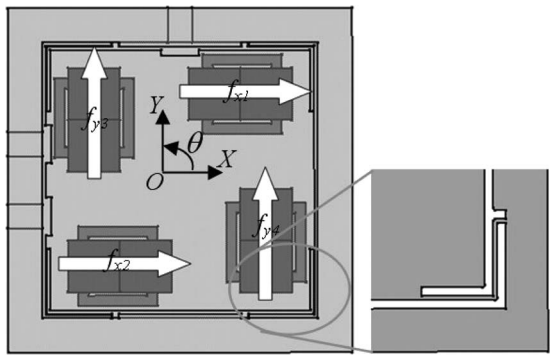

Fig. 2. Four sets of electromagnetic actuators and flexure mechanism.

A block diagram of the system is shown in Fig. 3. We can divide the system into two parts, hardware and software. There are several hardware blocks required. Now, we will model the electromagnetic actuators and the XY-flexure-mechanism dynamics based on Newton's motion law. There are also three software blocks. The measurement transformation is used to transform the measured signals into the real posture of the platen. The controller computes a wrench $w^d = [f_X \ f_Y \ \tau]^{\mathrm{T}}$ command to be generated by the actuators based on the desired trajectory and the real posture of the positioner. The force allocation block is needed to handle the redundancy of the force generation $F = [f_{x1} \ f_{x2} \ f_{y1} \ f_{y2}]^{\mathrm{T}}$, as four actuators are used to generate a 3×1 wrench. In the following, we will discuss each block.

A. Analysis of Magnetic-Force Characteristics

The electromagnetic actuator used is a VCM, which is a particular type of motor that provides linear motion. A VCM is used as the basic drive mechanism for faster and higher precision. Before starting the modeling process, several assumptions must be made for the purpose of simplification.

1) Referring to a coil design, the N-turn wires of the coils that are distributed over the cross section of each track are lumped as an equivalent single wire whose cross section is located at the center of that of the N-turn wires.
2) Each permanent magnet is viewed as a single turn of current-carrying wire wound around the side surface of the magnet.
3) The tracks are long enough with respect to the travel range of the moving part so that all the coils are only subject to uniform magnetic fields.
4) Each magnet is considered as one single magnetic dipole carrying the same magnetic dipole moment and is located at the center of each magnet.
5) The magnetic forces and torques between the magnets and coils can be linearized about the displacements in the X- and Y-directions.

In assumption 1), the force and torque characteristics of the lumped and the original models are not identical but are very similar [10]. In assumption 2), the volume current density of

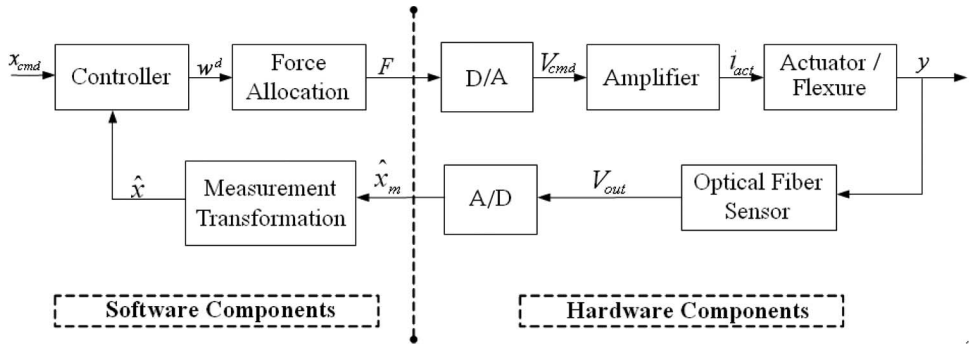

Fig. 3. Block diagram of the overall system.

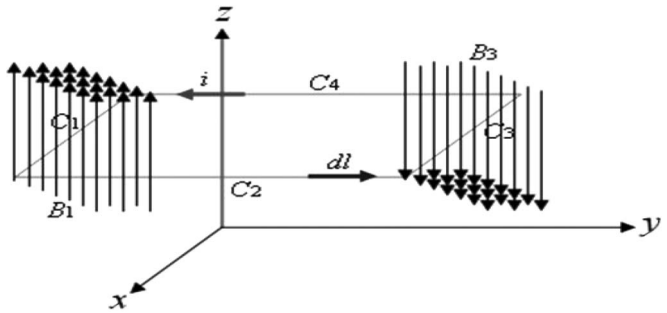

Fig. 4. Analysis of the magnetic force.

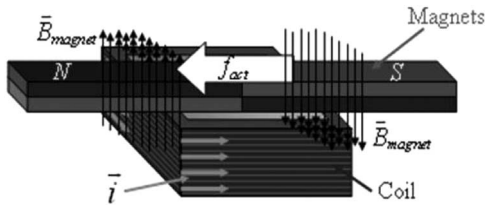

Fig. 5. Conceptual diagram of the electromagnetic actuator.

the permanent magnet is zero if it is uniformly magnetized; hence, only a surface current exists. Following assumption 1), assumption 2) is indirectly implied. Assumption 3) allows the magnetic field to be simply described by (1). Assumption 4) makes it feasible to employ and derive the nonlinear interaction forces and torques in this system. Finally, assumption 5) is reasonable when the mechanical structure is well designed.

Now, the force generated by the electromagnetic actuators will be analyzed. The Lorentz force principle expresses that, if a current-carrying conductor is placed in a magnetic field, a force will act upon it, which is proportional to the current and the magnetic flux density. Based on the assumptions, from Fig. 4, we can use one turn coil into four parts, i.e., C_1, C_2, C_3, and C_4, and define B_1, B_2, B_3, and B_4 as the magnetic flux density through each conducting wire. When the magnets are arranged in this way, only the two conducting wires C_1 and C_3 have magnetic field acting on them. Therefore, B_2 and B_4 can be assumed as zero. While the coil has N turns, the magnetic force of this actuator can be defined as

$$\begin{aligned} f &= \oint_C df \\ &= \oint_C idl \times B \\ &= \oint_{C1} idl_1 \times B_1 + \oint_{C2} idl_2 \times B_2 + \oint_{C3} idl_3 \times B_3 + \oint_{C4} idl_4 \times B_4 \\ &= iLB + 0 + iLB + 0 \\ &= 2iLB \end{aligned} \tag{1}$$

where B is defined as $B \equiv B_1 = B_3 = B_{\text{magnet}}$, i is a current carried on the conducting wires, and L is the edge length of the coil. If the coil has N turns, the force is

$$f_{\text{act}} = 2NLBi \equiv K_I i \tag{2}$$

where f_{act} means the actuated force and K_I is defined as the force constant.

For empirical justification, the magnetic force acting on the permanent magnet fixed beneath the moving part is shown in Fig. 5. Based on the magnetic-force analysis, Fig. 5 shows a conceptual diagram of a VCM. The VCM consists of two permanent magnets and one electromagnetic coil. The two permanent magnets are set in opposing directions to generate opposing magnetic fields $\vec{B}_{\text{magnet}}$, which, through the Lorentz force principle, create a force relative to the coil. Similar to the VCM principle, as the current flows through the coil along the counterclockwise direction, these permanent magnets will be forced to move to the left side. However, if the current flows along the clockwise direction, the permanent magnets will be forced to move to the right side. Therefore, using one set of this electromagnetic actuator, we can generate a single degree-of-freedom motion under a magnetic force $\vec{F}$. Since the two magnetic fields are in opposite directions, as are the currents through the opposite sides of the coil, where the magnetic fields interact with the current, the magnetic forces $\vec{F}$ on each side of the coil are in the same direction, i.e., the magnetic-force magnitude is twice as much as that obtained by a setup with one magnet and one coil.

The force relations between the actuators and platen are shown in Fig. 6. We define f_{x1}, f_{x2}, f_{y3}, and f_{y4} as the forces actuated by the nth actuator in the X- or Y-axis, respectively, and $w^d = [f_X^d \ f_Y^d \ \tau^d]^{\mathrm{T}}$ means that the force and torque are

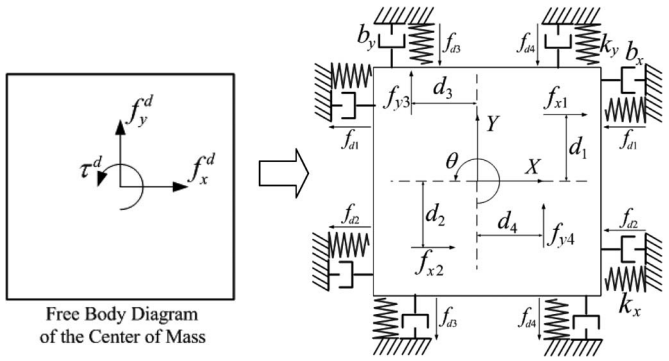

Fig. 6. Force relation between the actuators and platen.

really actuated in the center of mass. Therefore, the force kinematics is given by

$$\begin{bmatrix} f_x^d \\ f_y^d \\ \tau^d \end{bmatrix} = \begin{bmatrix} 1 & 1 & 0 & 0 \\ 0 & 0 & 1 & 1 \\ -d_1 & d_2 & -d_3 & d_4 \end{bmatrix} \begin{bmatrix} f_{x1} \\ f_{x2} \\ f_{y3} \\ f_{y4} \end{bmatrix} \tag{3}$$

where d_i, $i = 1$, 2, 3, and 4, denotes the distances from the center of the platen to the center of the actuators, as shown in Fig. 6.

However, every electromagnetic actuator has its limit to prevent the high generating power. Therefore, the saturation of the actuated force is determined by its maximum current $f_{\max} = K_I i_{\max}$. If each of the four actuators can generate up to a maximum force $f_{\max}$, then the wrench saturation constraints for the actuators are

$$\begin{aligned} &\left|f_X^d\right| \le 2f_{\max} \quad \left|f_Y^d\right| \le 2f_{\max} \\ &\left|\tau^d\right| \le 4f_{\max} d_m, \qquad d_m = \max(d_1, d_2, d_3, d_4). \end{aligned} \tag{4}$$

Due to the redundancy of the force generation, there are infinite solutions to satisfy these constraints. However, here, we choose the solution

$$\begin{bmatrix} f_{x1} \\ f_{x2} \\ f_{y3} \\ f_{y4} \end{bmatrix} = \begin{bmatrix} \frac{d_2}{d_1+d_2} & 0 & -\frac{1}{d_1+d_2} \\ \frac{d_1}{d_1+d_2} & 0 & \frac{1}{d_1+d_2} \\ 0 & \frac{d_4}{d_3+d_4} & -\frac{1}{d_3+d_4} \\ 0 & \frac{d_3}{d_3+d_4} & \frac{1}{d_3+d_4} \end{bmatrix} \begin{bmatrix} f_x^d \\ f_y^d \\ \tau^d \end{bmatrix}. \tag{5}$$

B. Dynamic Formulation

To develop the general model of this positioner, the coordinate is as defined in the previous section. Its origin is defined as the initial position of the positioner. The force relations are shown in Fig. 6. Here, we assume that the parallel flexure mechanism is a spring–mass damper system. Due to the symmetry of the flexure, the dynamics in the X- and Y-axes can be decoupled. Moreover, we also regard the hysteresis effect and thermal drift as the disturbances. By Newton's Law, the equations of the total forces and torques exerted on the platen can be expressed in the following:

$$\begin{aligned} \sum F_x &: M\ddot{x} = f_{x1} + f_{x2} - 2f_{d1} - 2f_{d2} - 4b_x\dot{x} \\ \sum F_y &: M\ddot{y} = f_{y3} + f_{y4} - 2f_{d3} - 2f_{d4} - 4b_y\dot{y} \\ \sum \tau_\theta &: I\ddot{\theta} = (-f_{x1} + 2f_{d1})d_1 + (f_{x2} - 2f_{d2})d_2 \\ &\quad + (-f_{y3} + 2f_{d3})d_3 \\ &\quad + (f_{y4} - 2f_{d4})d_4 - b_\theta\dot{\theta} \end{aligned} \tag{6}$$

where M and I are the mass and inertia of the platen and b_x, b_y, and b_θ are the damping constants.

On the other hand, the expressions of the displacements of the magnets x_1, x_2, y_3, and y_4 are as follows:

$$\begin{aligned} x_1 &= x - d_1\sin\theta \quad x_2 = x + d_2\sin\theta \\ y_3 &= y - d_3\sin\theta \quad y_4 = y + d_4\sin\theta. \end{aligned} \tag{7}$$

Since θ is a small angle of rotation, so that we may replace $\sin\theta$ by θ, the expressions of the four forces from the flexure mechanism can be obtained

$$\begin{aligned} f_{d1} &= k_x(x - d_1\theta) \quad f_{d2} = k_x(x + d_2\theta) \\ f_{d3} &= k_y(y - d_3\theta) \quad f_{d4} = k_y(y + d_4\theta) \end{aligned} \tag{8}$$

where k_x and k_y are the moduli of elasticity, whereas the actuated forces of each actuator are

$$\begin{aligned} f_{xn} &= K_I\, i_n, \qquad n = 1, 2 \\ f_{yn} &= K_I\, i_n, \qquad n = 3, 4 \end{aligned} \tag{9}$$

where i_1, i_2, i_3, and i_4 are the driven currents of each coil. Through the arrangement, we can get the following:

$$\begin{aligned} &\ddot{x} + \frac{4b_x}{M}\dot{x} + \frac{4k_x}{M}x - \frac{2k_x(d_1 - d_2)}{M}\theta = \frac{k_I}{M}(i_1 + i_2) \\ &\ddot{y} + \frac{4b_y}{M}\dot{y} + \frac{4k_y}{M}y - \frac{2k_y(d_3 - d_4)}{M}\theta = \frac{k_I}{M}(i_3 + i_4) \\ &\ddot{\theta} + \frac{b_\theta}{I}\dot{\theta} + \frac{2k_x\left(d_1^2 + d_2^2\right) + 2k_y\left(d_3^2 + d_4^2\right)}{I}\theta \\ &\quad - \frac{2k_x(d_1 - d_2)}{I}x - \frac{2k_y(d_3 - d_4)}{I}y \\ &\quad = \frac{-k_I}{I}(d_1 i_1 - d_2 i_2 + d_3 i_3 - d_4 i_4). \end{aligned} \tag{10}$$

Now, let the states be x, $\dot{x}$, y, $\dot{y}$, θ, and $\dot{\theta}$ and the outputs be x, y, and θ. Then, rearrange the aforementioned equations into the state-space form as

$$\begin{aligned} \dot{X} &= \bar{A}X + \bar{B}\bar{U} \\ Y &= \bar{C}X \end{aligned} \tag{11}$$

where

$$X = [\,x \quad \dot{x} \quad y \quad \dot{y} \quad \theta \quad \dot{\theta}\,]^{\mathrm{T}}$$
$$Y = [\,x \quad y \quad \theta\,]^{\mathrm{T}}$$
$$\bar{U} = [\,i_1 \quad i_2 \quad i_3 \quad i_4\,]^{\mathrm{T}}$$
$$\bar{A} = \begin{bmatrix} 0 & 1 & 0 & 0 & 0 & 0 \\ a_{x0} & a_{x1} & 0 & 0 & a_{x2} & 0 \\ 0 & 0 & 0 & 1 & 0 & 0 \\ 0 & 0 & a_{y0} & a_{y1} & a_{y2} & 0 \\ 0 & 0 & 0 & 0 & 0 & 1 \\ a_{\theta 0} & 0 & a_{\theta 1} & 0 & a_{\theta 2} & a_{\theta 3} \end{bmatrix}$$
$$a_{x0} = \frac{-4k_x}{M};\ a_{x1} = \frac{-4b_x}{M}$$
$$a_{x2} = \frac{2k_x(d_1 - d_2)}{M};\ a_{y0} = \frac{-4k_y}{M}$$
$$a_{y1} = \frac{-4b_y}{M};\ a_{y2} = \frac{2k_y(d_3 - d_4)}{M}$$
$$a_{\theta 0} = \frac{2k_x(d_1 - d_2)}{I};\ a_{\theta 1} = \frac{2k_y(d_3 - d_4)}{I}$$
$$a_{\theta 2} = \frac{-2k_x\left(d_1^2 - d_2^2\right) - 2k_y\left(d_3^2 - d_4^2\right)}{I}$$
$$a_{\theta 3} = \frac{-b_\theta}{I}$$
$$\bar{B} = \begin{bmatrix} 0 & 0 & 0 & 0 \\ \frac{k_I}{M} & \frac{k_I}{M} & 0 & 0 \\ 0 & 0 & 0 & 0 \\ 0 & 0 & \frac{k_I}{M} & \frac{k_I}{M} \\ 0 & 0 & 0 & 0 \\ \frac{-k_I d_1}{I} & \frac{k_I d_2}{I} & \frac{-k_I d_3}{I} & \frac{k_I d_4}{I} \end{bmatrix}$$
$$\bar{C} = \begin{bmatrix} 1 & 0 & 0 & 0 & 0 & 0 \\ 0 & 0 & 1 & 0 & 0 & 0 \\ 0 & 0 & 0 & 0 & 1 & 0 \end{bmatrix}.$$

III. Controller Design

In the modeling process, we have made some assumptions that will lead to some modeling errors. Moreover, an electromagnetic system also meets parameter variations such as magnetization drifting and air-gap coupling that need to be effectively suppressed for precision motion control. Therefore, the stabilizing controller developed here should be robust enough to tolerate these inherent uncertainties.

So far, there are several available control methodologies to overcome modeling uncertainties and to reject external disturbances, particularly in the field of robust controllers, including H^∞ control, linear–quadratic–Gaussian control, sliding mode control, fuzzy control, backstepping control, and so on. These controller gains are mostly fixed and designed according to the nominal model. Based on one of such robust control schemes, the resulting controller is sufficiently robust to the modeling uncertainty. However, there also exist some drawbacks; for example, this controller will probably fail if the changes of the plant's dynamics behavior exceed the controller's tolerance. In this paper, to attain the capability of online gain tuning as well as robustness [42], we intend to combine the adaptive and robust controllers [43]. Hence, we propose an ASMC in this paper.

Referring to the plant model of (11), we impose a special case which requires that the rotation angle θ must be held zero when the platen is actuated. Therefore, the torque must equal zero all the time, and the actuated forces should satisfy the following: $f_{x1} = f_{x2}$ and $f_{y1} = f_{y2}$. However, we fail to have a perfect assembly of the actuator and mechanism; therefore, we add one rotational control effort u_θ to compensate the assembling errors. Therefore, the plant's model can be rewritten as follows:

$$\begin{aligned} \ddot{x} + a_{x1}\dot{x} + a_{x0}x &= 2K_u u_x \\ \ddot{y} + a_{y1}\dot{y} + a_{y0}y &= 2K_u u_y \\ \ddot{\theta} + a_{\theta 1}\dot{\theta} + a_{\theta 0}\theta &= u_\theta. \end{aligned} \tag{12}$$

Therefore, the distribution of the control efforts can be assigned as follows:

$$\begin{aligned} u_1 &= u_x + u_\theta \quad u_2 = u_x \\ u_3 &= u_y - u_\theta \quad u_4 = u_y. \end{aligned} \tag{13}$$

In the following, define the state variables $x_1 = x$, $x_2 = \dot{x}$, $y_1 = y$, $y_2 = \dot{y}$, $\theta_1 = \theta$, and $\theta_2 = \dot{\theta}$. Moreover, the desired position command is defined as x_{1d}, y_{1d}, and θ_{1d}. Then, the system dynamics can be transformed into error coordinates using the relations $\tilde{x}_1 = x_1 - x_{1d}$, $\tilde{x}_2 = x_2 - x_{2d}$, $\tilde{y}_1 = y_1 - y_{1d}$, $\tilde{y}_2 = y_2 - y_{2d}$, $\tilde{\theta}_1 = \theta_1 - \theta_{1d}$, and $\tilde{\theta}_2 = \theta_2 - \theta_{2d}$. Use the compact notations $E \equiv [\tilde{x}\ \tilde{y}\ \tilde{\theta}]^{\mathrm{T}}$ and $X_d \equiv [x_{1d}\ y_{1d}\ \theta_{1d}]^{\mathrm{T}}$. The error equation can be defined as follows:

$$\ddot{E} = AX + BU - \ddot{X}_d \tag{14}$$

where

$$X \equiv [\,x_1 \quad x_2 \quad y_1 \quad y_2 \quad \theta_1 \quad \theta_2\,]^{\mathrm{T}}$$
$$U \equiv [\,u_x \quad u_y \quad u_\theta\,]^{\mathrm{T}}$$
$$A = \begin{bmatrix} a_{x0} & a_{x1} & 0 & 0 & a_{x2} & 0 \\ 0 & 0 & a_{y0} & a_{y1} & a_{y2} & 0 \\ a_{\theta 0} & 0 & a_{\theta 1} & 0 & a_{\theta 2} & a_{\theta 3} \end{bmatrix}$$
$$B = \begin{bmatrix} \frac{2k_I}{M} & 0 & \frac{k_I}{M} \\ 0 & \frac{2k_I}{M} & \frac{k_I}{M} \\ \frac{-k_I(d_1 - d_2)}{I} & \frac{-k_I(d_3 - d_4)}{I} & \frac{k_I(d_2 + d_4)}{I} \end{bmatrix}.$$

From the system matrix A, it is obvious that, if d_1 is exactly equal to d_2, then x and θ are decoupled. Similarly, if d_3 is exactly equal to d_4, then y and θ are also decoupled. Here, we can see it as three single-input single-output systems. Nevertheless, we have made some assumptions for the simplification of the system plant's development, and hence, those assumptions may result in some inaccuracies of the plant model. Thus, disturbance terms need to be added into the plant model. Then, the uncertainty term can be divided into two parts, i.e., one is a constant uncertainty W_{const} and the other one is a varying uncertainty W_{var}. Therefore, (14) can be expressed as

$$\ddot{E} = AX + BU - \ddot{X}_d + W_{\mathrm{const}} + W_{\mathrm{var}} \tag{15}$$

and the varying uncertainty is bounded and satisfies $\|W_{\mathrm{var}}\| \leq W_{\mathrm{MAX}}$.

A. Controller Design

Assume a sliding surface S with the following form:

$$S = \dot{E} + \Lambda E \tag{16}$$

where $\Lambda \equiv \mathrm{diag}[\lambda_1\ \lambda_2\ \lambda_3]$ is designed as a positive diagonal matrix. We try to regulate state error E to zero which simultaneously regulates the derivative of E to zero. Due to this reason, if it can be proven that the sliding surface tends to zero within finite time, then E and $\dot{E}$ are also forced to zero exponentially. To relate the sliding surface to the dynamics of motion, the time derivative of the sliding surface can be found out

$$\dot{S} = \ddot{E} + \Lambda \dot{E}. \tag{17}$$

As described in the previous section, an adaptive controller is applied in this paper, which is capable of estimating parameters of the system online while controlling the system simultaneously. After we have the estimates of the system parameters, (17) with these estimates in the control command can be used. Therefore, we substitute the estimates acquired from the online estimator and derive the control command as

$$U_{\mathrm{AS}} = \hat{B}^{-1}\Big(-AX + \ddot{X}_d - \Lambda\dot{E} - \hat{W}_{\mathrm{const}} - KS - N\mathrm{sat}(S)\Big) \tag{18}$$

where $K \equiv \mathrm{diag}[k_1\ k_2\ k_3]\ \forall k_i > 0$, $N \equiv \mathrm{diag}[\eta_1\ \eta_2\ \eta_3]\ \forall \eta_i > 0$, $\hat{B}$ and $\hat{W}_{\mathrm{const}}$ are the estimated values of B and W_{const}, respectively, and $\mathrm{sat}(\cdot)$ is the saturation function

$$\mathrm{sat}(S) = \begin{cases} 1 & S > \varepsilon \\ \frac{S}{|\varepsilon|} & \text{if } \varepsilon \geq S \geq -\varepsilon \\ -1 & S < -\varepsilon \end{cases} \tag{19}$$

where ε is the width of the boundary layer. Substituting (18) into (16), we can obtain

$$\begin{aligned} \ddot{E} &= AX + B\left[\hat{B}^{-1}\left(-AX + \ddot{X}_d - \Lambda\dot{E} \right.\right. \\ &\qquad \left.\left. -\hat{W}_{\mathrm{const}} - KS - N\mathrm{sat}(S)\right)\right] \\ &\quad - \ddot{X}_d + W_{\mathrm{const}} + W_{\mathrm{var}} \\ &= AX + (\tilde{B} + \hat{B})\left[\hat{B}^{-1}\left(-AX + \ddot{X}_d - \Lambda\dot{E} \right.\right. \\ &\qquad \left.\left. -\hat{W}_{\mathrm{const}} - KS - N\mathrm{sat}(S)\right)\right] \\ &\quad - \ddot{X}_d + W_{\mathrm{const}} + W_{\mathrm{var}} \\ &= \tilde{B}U_{\mathrm{AS}} - \Lambda\dot{E} - KS - N\mathrm{sat}(S) + \tilde{W}_{\mathrm{const}} + W_{\mathrm{var}} \end{aligned} \tag{20}$$

where the estimation errors are defined as $\tilde{B} = B - \hat{B}$ and $\tilde{W}_{\mathrm{const}} = W_{\mathrm{const}} - \hat{W}_{\mathrm{const}}$. By applying appropriate gains K, N, and Λ, we can accelerate the convergence and force the system states to zero in a shorter period of time.

B. Stability Analysis

Define a Lyapunov function candidate V, which is a positive definite function

$$V = \frac{1}{2}S^{\mathrm{T}}S + \frac{1}{2}\mathrm{tr}\left(\tilde{B}^{\mathrm{T}}\Gamma_1^{-1}\tilde{B}\right) + \frac{1}{2}\mathrm{tr}\left(\tilde{W}_{\mathrm{const}}^{\mathrm{T}}\Gamma_2^{-1}\tilde{W}_{\mathrm{const}}\right) \tag{21}$$

where Γ_1^{-1} and Γ_2^{-1} are all positive diagonal matrices. First, the time derivative of the Lyapunov candidate function V can be found out as

$$\dot{V} = S^{\mathrm{T}}\dot{S} + \mathrm{tr}\left(\tilde{B}^{\mathrm{T}}\Gamma_1^{-1}\dot{\tilde{B}}\right) + \mathrm{tr}\left(\tilde{W}_{\mathrm{const}}^{\mathrm{T}}\Gamma_2^{-1}\dot{\tilde{W}}_{\mathrm{const}}\right). \tag{22}$$

As described in (17)–(21), (23) can be expressed as

$$\begin{aligned} \dot{V} = &-S^{\mathrm{T}}KS - S^{\mathrm{T}}\left(N\mathrm{sat}(S) - W_{\mathrm{var}}\right) + S^{\mathrm{T}}\tilde{B}U_{\mathrm{AS}} \\ &+ S^{\mathrm{T}}\tilde{W}_{\mathrm{const}} + \mathrm{tr}\left(\tilde{B}^{\mathrm{T}}\Gamma_1^{-1}\dot{\tilde{B}}\right) + \mathrm{tr}\left(\tilde{W}_{\mathrm{const}}^{\mathrm{T}}\Gamma_2^{-1}\dot{\tilde{W}}_{\mathrm{const}}\right). \end{aligned} \tag{23}$$

In order to further manipulate (23) we can rewrite the third and fourth terms on the right-hand side of (23) as

$$\begin{aligned} S^{\mathrm{T}}\tilde{B}U_{\mathrm{AS}} &= \left((S^{\mathrm{T}}\tilde{B})^{\mathrm{T}}\right)^{\mathrm{T}}U_{\mathrm{AS}} = \mathrm{tr}\left[(S^{\mathrm{T}}\tilde{B})^{\mathrm{T}}U_{\mathrm{AS}}^{\mathrm{T}}\right] \\ &= \mathrm{tr}\left(\tilde{B}^{\mathrm{T}}SU_{\mathrm{AS}}^{\mathrm{T}}\right) \\ S^{\mathrm{T}}\tilde{W}_{\mathrm{const}} &= \mathrm{tr}\left(\tilde{W}_{\mathrm{const}}^{\mathrm{T}}S\right). \end{aligned} \tag{24}$$

Hence, by rearranging (23), we can get the following:

$$\begin{aligned} \dot{V} = &-S^{\mathrm{T}}KS - S^{\mathrm{T}}\left(N\mathrm{sat}(S) - W_{\mathrm{var}}\right) \\ &+ \mathrm{tr}\left[\tilde{B}^{\mathrm{T}}\left(\Gamma_1^{-1}\dot{\tilde{B}} + SU_{\mathrm{AS}}^{\mathrm{T}}\right)\right] \\ &+ \mathrm{tr}\left[\tilde{W}_{\mathrm{const}}^{\mathrm{T}}\left(\Gamma_2^{-1}\dot{\tilde{W}}_{\mathrm{const}} + S\right)\right]. \end{aligned} \tag{25}$$

Now, the adaptive laws are designed in the following:

$$\dot{\hat{B}} = -\dot{\tilde{B}} = \Gamma_1 SU_{\mathrm{AS}}^{\mathrm{T}} \tag{26}$$

$$\dot{\hat{W}}_{\mathrm{const}} = -\dot{\tilde{W}}_{\mathrm{const}} = \Gamma_2 S. \tag{27}$$

In order to maintain stability and to prevent saturation of the control effort, $\hat{B}$ must be bounded away from zero in (18). One method to avoid $\hat{B}$ going through zero is to modify the adaptive law using a projection method. Such a modification does not affect the convergence of $\tilde{B}$ and is achieved by using prior knowledge of B, such that $B \geq B(t_0)$, where $B(t_0)$ is defined as the lower bound. Applying the projection method to the adaptive law, we obtain

$$\dot{\hat{B}}(t) = \begin{cases} \Gamma_1 SU_{\mathrm{AS}}^{\mathrm{T}} & \text{if } \hat{B}(t) \geq B(t_0) \\ 0 & \text{otherwise.} \end{cases} \tag{28}$$

At the initial time, $\hat{B}(t_0)$ is chosen so that $\hat{B}(t_0) > B(t_0)$. Substitute adaptive and projection laws into (26), and then

$$\begin{aligned} \dot{V} = &-S^{\mathrm{T}}KS - S^{\mathrm{T}}\left(N\mathrm{sat}(S) - W_{\mathrm{var}}\right) \\ &+ \mathrm{tr}\left[\tilde{B}^{\mathrm{T}}\left(\Gamma_1^{-1}\left(-\Gamma_1 SU_{\mathrm{AS}}^{\mathrm{T}}\right) + SU_{\mathrm{AS}}^{\mathrm{T}}\right)\right] \\ &+ \mathrm{tr}\left[\tilde{W}_{\mathrm{const}}^{\mathrm{T}}\left(\Gamma_2^{-1}(-\Gamma_2 S) + S\right)\right] \\ = &-S^{\mathrm{T}}KS - S^{\mathrm{T}}\left(N\mathrm{sat}(S) - W_{\mathrm{var}}\right) \end{aligned} \tag{29}$$

because K is a positive diagonal matrix and the norm of matrix N is designed to be larger than the upper bound of the varying uncertainty W_{var}, i.e., $\|N\| \geq |W_{\mathrm{var}}\|$, and thus, they are commutable in deriving the inequality. Equation (29)

TABLE I
SPECIFICATIONS OF SETUP

CPU	Pentium IV 2.4 G*Hz*
Operating System	Windows XP
Controller language	Matlab Real-Time Target Ver.2.5.1
D/A &A/D card	NI 6733 (16 bits), NI 6034E (16 bits)
Power Amplifier	ADP-055-18 (*Copley*)
Measurement system	1. Z4W-V (Omron) 2. homemade fiber interferometer
Coil	360 turns, d=0.3mm, 50×50×10 mm^3
Permanent magnet	NdfeB, 50×10×3 mm^3
Positioner dimension	100×100×30 mm^3

also implies that the equilibriums $B = \hat{B}$ and $W_{\text{const}} = \hat{W}_{\text{const}}$ of the respective equations are uniformly bounded. Using the arguments similar to Barbalat's Lemma, we establish that $S \in L_2$, $\dot{S} \in L_\infty$, and $|S(t)| \to 0$. Furthermore, if the persistence of excitation holds, then $\|\tilde{B}\| \to 0$ and $\|\tilde{W}_{\text{const}}\| \to 0$ as $t \to \infty$.

Due to the convergence to zero of S, it can be readily verified that E converges to zero asymptotically. In other words, state variables and their time derivatives all converge to zero eventually, which is the goal of designing the controller for this system.

IV. EXPERIMENTAL RESULTS

The experimental hardware, including the main body, sensor system, driver system, and controller hardware will be described here (Table I). A number of experimental results, including the regulation, step test, and sinusoidal motion tracking will also be provided in this section to demonstrate the performance of this system with the ASMC.

A. Experimental Hardware

To make the positioner compact and to utilize the advantages of monolithic construction, the flexure mechanism stage was manufactured by using precision wire electrical discharge machining. For the reason of avoiding the electromagnetic interference effects, the requirement of larger travel range, and high resolution, the optical sensor and homemade fiber interferometer are therefore chosen in this experiment, which can test and verify the different situations of moving range. Due to the budget, first, we use the Z4W-V optical sensor, manufactured by *OMRON*, Japan, with 10-kHz sampling frequency, 8-mm active range, 5° maximum angular vision range, and 5-μm accuracy to verify the fast response ability of the positioner. Second, the homemade fiber interferometers are used to demonstrate the resolution to submicrometric. Its active range is up to 1 mm, and the accuracy is of $\pm$165 nm. However, its limitation is the maximum velocity and sampling frequency. Due to the limitation of the bandwidth of the fiber interferometer, the maximum velocity of the system is held at 100 μm/s. The whole hardware of the compact positioner is shown in Fig. 7. The figure shows that three homemade fiber interferometers are mounted on the positioner and three commercial optical sensors are placed on the symmetric positions, which are opposite to the fiber interferometers. The power driver type is an ADP-055-18 torque amplifier which is manufactured by *Copley Controls Corporation* in the U.S. They are linear drivers designed to be servo drivers for dc motors. The continuous output power is 0.33 W with an input voltage of 20–55 V. The current microcomputer is an IBM PC with a Pentium IV microprocessor inside. The clock rate is 2.4 GHz which allows this research to accomplish a real-time control implementation. The type of analog–digital converter is a 16-b high-resolution data acquisition adapter (NI 6034E), and the type of digital–analog converter is altogether six converting channels with 16-b resolution each (NI 6733). Based on the experimental results, a sampling time between 0.1 and 0.05 ms leads to a better behavior of this system.

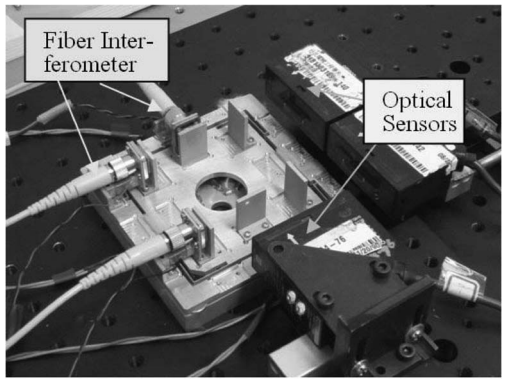

Fig. 7. Experimental device of the positioner.

B. System Performance

1) Transient Response With Largest Displacement: In order to test the large moving range (millimeter-level) capability of this system, we execute the X-axis positioning motion and let the other two states be regulated to zero, i.e., we set the control goal as to eventually converge these configuration states to the point at $x = 0.5$ mm, $y = 0$ mm, and $\theta = 0°$. We set the desired trajectory to be represented by a black thin line, and the actual trajectory for the SMC is represented by a gray dotted line and that for the ASMC is represented by a black bold line. First, we set the (SMC) parameters $\Lambda = \text{diag}[5\ 4.5\ 2.3]$, and then, the configuration states converge to the set point. From Fig. 8, the configuration states in the X-axis can converge to the desired points within 0.9 s. Moreover, this figure reveals that the instant motion on the XY plane will have great influences on the other two states that are not acceptable in most applications. In other words, the robustness of this proposed SMC is not sufficient, and thus, the ASMC is expected to overcome this shortcoming. For the ASMC, the configuration states in the X-axis can converge to the desired points in 0.25 s, and the other two states in the Y- and Z_θ-axes become stable in 0.3 s. Due to the property of higher robustness that the ASMC possesses, the coupling influences existing on the other two configuration states, namely, y and θ, become dramatically small and within acceptable ranges. The steady-state error is below ± 5 μm which is satisfactory for a commercial optical sensor.

2) Tracking Response: A step-train motion is one of the most common operations of the positioning systems in industries. For the purpose of maintaining the high-quality processing of the material pieces, ICs, or products, this kind of motion

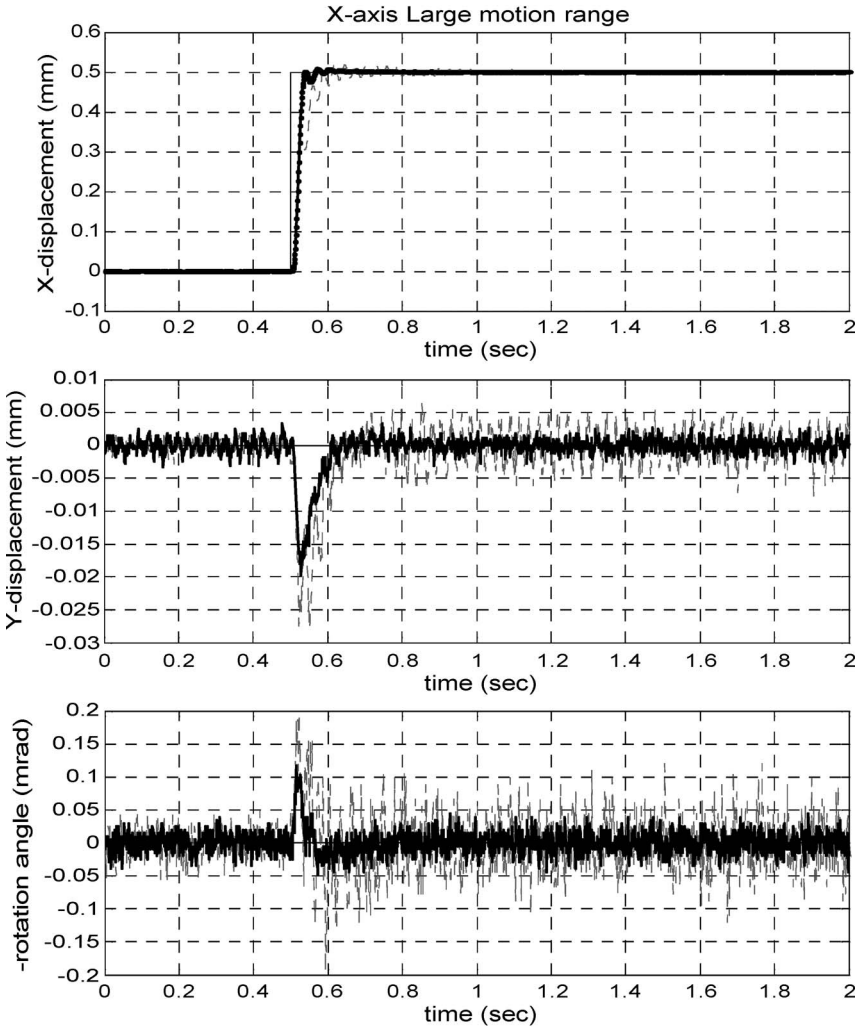

Fig. 8. Large moving range $+0.5$ mm in the X-axis.

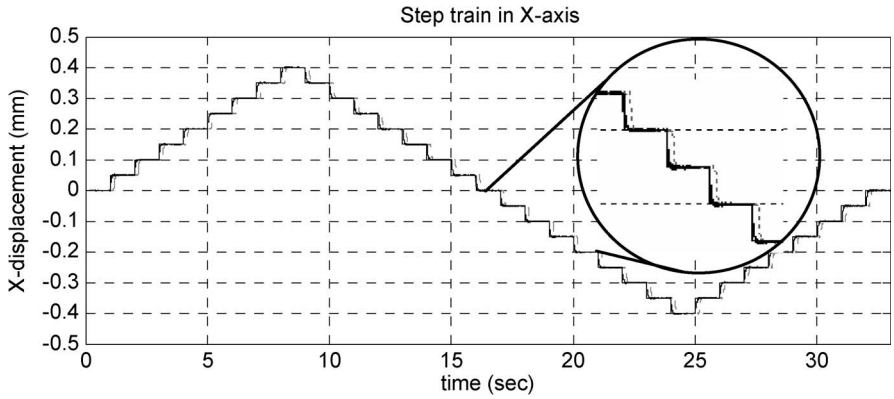

Fig. 9. Step-train response in the X-axis.

is extraordinarily important. Therefore, in order to validate the feasibility in practical applications, a subsequent step-response experiment, with each step equal to 50 μm and moving toward ± 0.4 mm, has been conducted. The experimental result, as shown in Fig. 9, demonstrates this satisfactorily. From this figure, SMC and ASMC can similarly achieve the transient time within 0.05 s and the final steady-state errors within the resolution level of the detecting sensors.

To illustrate the tracking capability for the proposed positioner, we will present the experimental results of the sinusoidal motion with the amplitude equal to ± 0.2 mm at the lower frequency of 0.25 Hz and higher frequency of 2 Hz, respectively. Fig. 10 shows the fine tracking ability on the XY plane. For ASMC, the rms of the tracking error is 5.9 μm, and the time lag is very small, but for the SMC, the rms of tracking error is 7.5 μm, and the time lag is existed. As we continue to increase

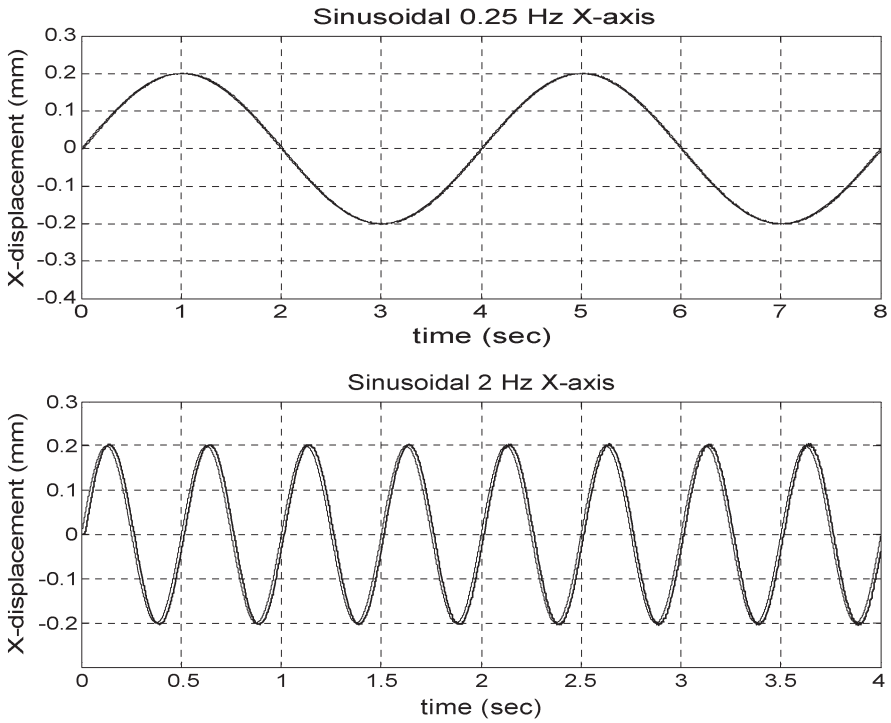

Fig. 10. Sinusoidal motion.

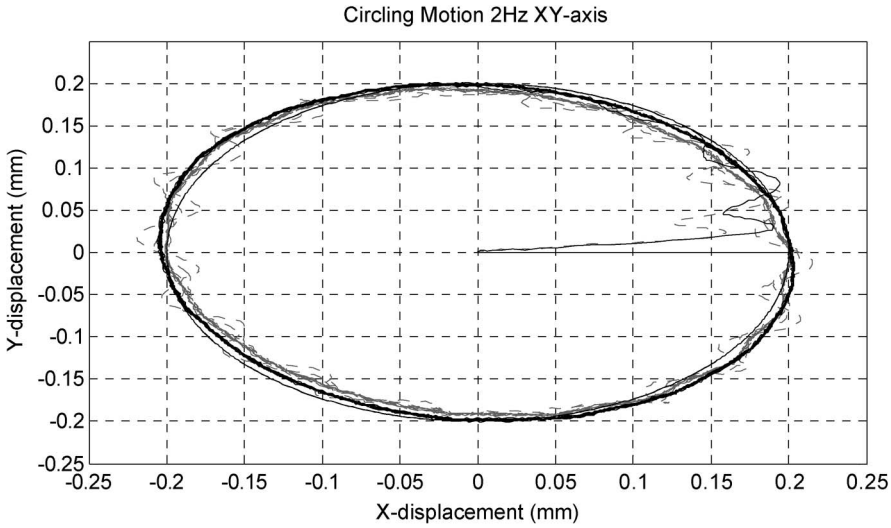

Fig. 11. Circling motion at 0.5 Hz.

the frequency of the desired motion to 2 Hz, the experiment remains satisfactory of ASMC, as shown in Fig. 10, but for the SMC, the tracking error and time lag are lager than the slower frequency. The other way to show the tracking and contouring capability is to profile a desired circle. The experimental results of this circling motion with radius equal to ± 0.2 mm at a frequency of 0.25 Hz is shown in Fig. 11. It shows the fine tracking ability on the XY plane. For the SMC, the trajectory has chattering along the desired circle. For the ASMC, the trajectory traversed by the platen almost perfectly overlaps the desired circle. The rms value of contour error for the ASMC is 20.675 μm.

Next, we use the homemade fiber interferometer as sensor to feedback the positioning information. In the following, we make a series of regulation motion from 5 to 100 μm, as shown in Fig. 12, and the steady-state error can be achieved at ± 165 nm. Based on the experimental results, satisfactory performance including stiffness and high resolution has been achieved by ASMC. This validates the design of the system hardware and demonstrates the feasibility of the developed controller.

V. Conclusion

In this paper, we have integrated an XY-axis flexure mechanism and electromagnetic actuators into a novel 3-DOF submicropositioner with larger travel range. The dynamics of the positioner has been thoroughly analyzed, and then, a complete model has also been derived. An adaptive SMC has been

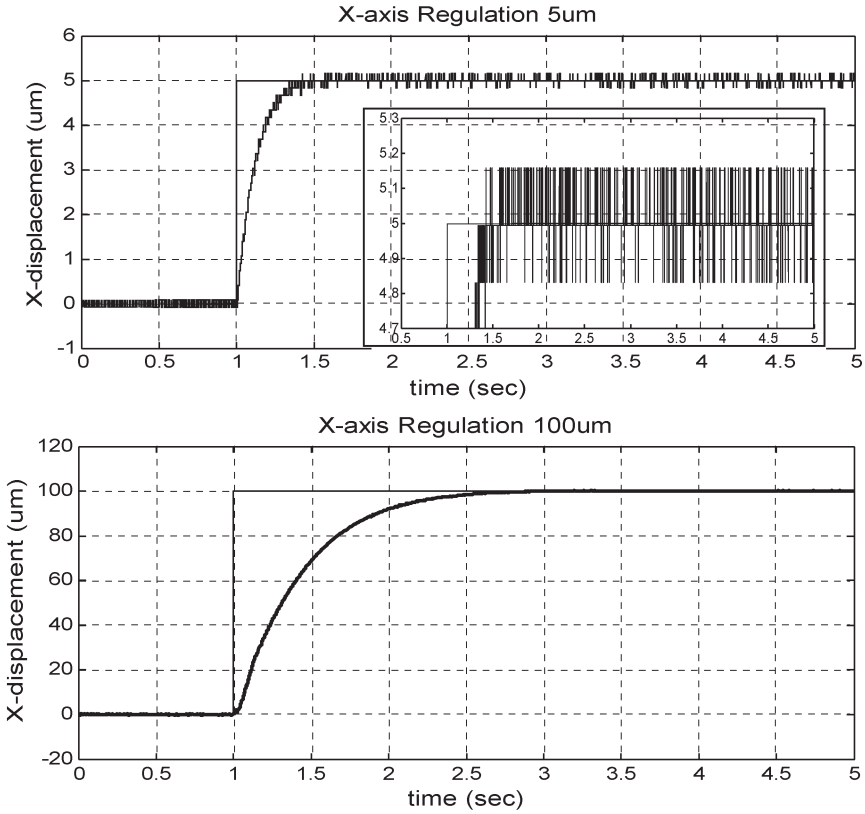

Fig. 12. Regulation motion from 5 to 100 μm.

designed here and implemented using a microcomputer. In the experimental results, the proposed ASMC, which can perform online system identification implicitly or explicitly while tuning the controller gains, can really guarantee the stability, regulation, and tracking of the closed-loop system. At the same time, the good performance can reveal that the three objectives, i.e., larger travel range, precision positioning, and more compact structure, are achieved.

ACKNOWLEDGMENT

The authors' gratitude goes to the Academic Paper Editing Clinic, NTNU.

REFERENCES

[1] L. Marton and B. Lantos, "Modeling, identification, and compensation of stick-slip friction," *IEEE Trans. Ind. Electron.*, vol. 54, no. 1, pp. 511–521, Feb. 2007.

[2] M. L. Corradini and G. Orlando, "Robust stabilization of nonlinear uncertain plants with backlash or dead zone in the actuator," *IEEE Trans. Control Syst. Technol.*, vol. 10, no. 1, pp. 158–166, Jan. 2002.

[3] M.-F. Hsieh, C.-J. Tung, W.-S. Yao, M.-C. Wu, and Y.-S. Liao, "Servo design of a vertical axis drive using dual linear motors for high speed electric discharge machining," *Int. J. Mach. Tools Manuf.*, vol. 47, no. 3/4, pp. 546–554, Mar. 2007.

[4] R. Martinez, J. Alvarez, and Y. Orlov, "Hybrid sliding-mode-based control of underactuated systems with dry friction," *IEEE Trans. Ind. Electron.*, vol. 55, no. 11, pp. 3998–4003, Nov. 2008.

[5] T. Galante, J. E. Frank, J. Bernard, W. Chen, G. A. Lesieutre, and G. H. Koopmann, "Design, modeling, and performance of a high-force piezoelectric inchworm motor," in *Proc. Smart Struct. Integr. Syst.*, 1998, vol. 3329, pp. 756–767.

[6] P. E. Tenzer and R. B. Mrad, "A systematic procedure for the design of piezoelectric inchworm precision positioners," *IEEE/ASME Trans. Mechatronics*, vol. 9, no. 2, pp. 427–435, Jun. 2004.

[7] J. Y. Shim and D. G. Gweon, "Piezo-driven metrological multiaxis nanopositioner," *Rev. Sci. Instrum.*, vol. 72, no. 11, pp. 4183–4187, Nov. 2001.

[8] K. S. J. Pister, R. S. Fearing, and R. T Howe, "A planar air levitated electrostatic actuator system," in *Proc. IEEE Investigation Micro Struct. Sens., Actuators, Mach. Robots*, 1990, pp. 67–71.

[9] X. Shan, S. K. Kuo, J. Zhang, and C. H. Menq, "Ultra precision motion control of a multiple degrees of freedom magnetic suspension stage," *IEEE/ASME Trans. Mechatronics*, vol. 7, no. 1, pp. 67–78, Mar. 2002.

[10] W. J. Kim, D. L. Trumper, and J. H. Lang, "Modeling and vector control of planar magnetic levitator," *IEEE Trans. Ind. Appl.*, vol. 34, no. 6, pp. 1254–1262, Nov./Dec. 1998.

[11] S. Salapaka, "Control of the nanopositioning devices," in *Proc. Conf. Decision Control*, 2003, pp. 3644–3649.

[12] S. Bashash and N. Jalili, "Robust adaptive control of coupled parallel piezo-flexural nanopositioning stages," *IEEE/ASME Trans. Mechatronics*, vol. 14, no. 1, pp. 11–20, Feb. 2009.

[13] D. Oetomo, D. Daney, B. Shirinzadeh, and J.-P. Merlet, "Certified workspace analysis of 3RRR planar parallel flexure mechanism," in *Proc. IEEE Int. Conf. Robot. Autom.*, 2008, pp. 3838–3843.

[14] H.-H. Pham, I.-M. Chen, and H.-C. Yeh, "Micro-motion selective-actuation X Y Z flexure parallel mechanism: Design and modeling," *J. Micromechatronics*, vol. 3, no. 1, pp. 51–73, 2005.

[15] Y. Tian, B. Shirinzadeh, and D. Zhang, "A flexure-based mechanism and control methodology for ultra-precision turning operation," *Precis. Eng.*, vol. 33, no. 2, pp. 160–166, Apr. 2009.

[16] S. O. R. Moheimani, "A survey of recent innovations in vibration damping and control using shunted piezoelectric transducers," *IEEE Trans. Control Syst. Technol.*, vol. 11, no. 4, pp. 482–494, Jul. 2003.

[17] E. K. Akdogan, M. Allahverdi, and A. Safari, "Piezoelectric composites for sensor and actuator applications," *IEEE Trans. Ultrason., Ferroelectr., Freq. Control*, vol. 52, no. 5, pp. 746–775, May 2005.

[18] H.-J. Shieh and C.-H. Hsu, "An adaptive approximator-based backstepping control approach for piezoactuator-driven stages," *IEEE Trans. Ind. Electron.*, vol. 55, no. 4, pp. 1729–1738, Apr. 2008.

[19] Products P-780, Physik Instrumente Product Catalog2005.

[20] S. Verma, W.-J. Kim, and H. Shakir, "Multi-axis maglev nanopositioner for precision manufacturing and manipulation applications," *IEEE Trans. Ind. Appl.*, vol. 41, no. 5, pp. 1159–1167, Sep./Oct. 2005.

[21] P. Samanta and H. Hirani, "Magnetic bearing configurations: Theoretical and experimental studies," *IEEE Trans. Magn.*, vol. 44, no. 2, pp. 292–300, Feb. 2008.
[22] O.-S. Kim, S.-H. Lee, and D.-C. Han, "Positioning performance and straightness error compensation of the magnetic levitation stage supported by the linear magnetic bearing," *IEEE Trans. Ind. Electron.*, vol. 50, no. 2, pp. 374–378, Apr. 2003.
[23] J. Zhu, H. Lu, Y. Guo, and Z. Lin, "Development of electromagnetic linear actuators for micro robots," in *Proc. Int. Conf. Elect. Mach. Syst.*, 2008, pp. 3673–3679.
[24] P. Fang, F. Ding, Q. Li, and Y. Li, "High-response electromagnetic actuator with twisting axis for gravure systems," *IEEE Trans. Magn.*, vol. 45, pt. 1, no. 1, pp. 172–176, Jan. 2009.
[25] L. Petit, C. Prelle, E. Dore, F. Lamarque, and M. Bigerelle, "Optimized design of a four discrete positions electromagnetic actuator," in *Proc. IEEE Int. Conf. Mechatronics*, 2009.
[26] Y. Fujimoto, T. Kominami, and H. Hamada, "Development and analysis of a high thrust force direct-drive linear actuator," *IEEE Trans. Ind. Electron.*, vol. 56, no. 5, pp. 1383–1392, May 2009.
[27] E. Fitan, F. Messine, and B. Nogarede, "The electromagnetic actuator design problem: A general and rational approach," *IEEE Trans. Magn.*, vol. 40, no. 3, pp. 1579–1590, May 2004.
[28] M.-Y. Chen, H.-W. Tzeng, and S.-K. Hung, "A new mechanism design of electro-magnetic actuator for a micro-positioner," *ISA Trans.*, vol. 46, no. 1, pp. 41–48, Feb. 2007.
[29] M. Reyhanoglu and S. Drakunov, "Attitude stabilization of small satellites using only magnetic actuation," in *Proc. 34th IEEE IECON*, Nov. 2008, pp. 103–107.
[30] A. Forrai, T. Ueda, and T. Yumura, "Electromagnetic actuator control: A linear parameter-varying (LPV) approach," *IEEE Trans. Ind. Electron.*, vol. 54, no. 3, pp. 1430–1441, Jun. 2007.
[31] A. D. Yalcinkaya, H. Urey, D. Brown, T. Montague, and R. Sprague, "Two-axis electromagnetic microscanner for high resolution displays," *J. Microelectromech. Syst.*, vol. 15, no. 4, pp. 786–794, Aug. 2006.
[32] C.-H. Ji, M. Choi, S.-C. Kim, K.-C. Song, J.-U. Bu, and H.-J. Nam, "Electromagnetic two-dimensional scanner using radial magnetic field," *J. Microelectromech. Syst.*, vol. 16, no. 4, pp. 989–996, Aug. 2007.
[33] X.-K. Chen and T. Hisayama, "Adaptive sliding-mode position control for piezo-actuated stage," *IEEE Trans. Ind. Electron.*, vol. 55, no. 11, pp. 3927–3934, Nov. 2008.
[34] A. Sabanovic, M. Elitas, and K. Ohnishi, "Sliding modes in constrained systems control," *IEEE Trans. Ind. Electron.*, vol. 55, no. 9, pp. 3332–3339, Sep. 2008.
[35] Q. Hu, C.-L. Du, L.-H. Xie, and Y.-Y. Wang, "Discrete-time sliding mode control with time-varying surface for hard disk drives," *IEEE Trans. Control Syst. Technol.*, vol. 17, no. 1, pp. 175–183, Jan. 2009.
[36] K. Abidi and A. Sabanovic, "Sliding-mode control for high-precision motion of a piezostage," *IEEE Trans. Ind. Electron.*, vol. 54, no. 1, pp. 629–637, Feb. 2007.
[37] M. O. Efe, "Fractional fuzzy adaptive sliding-mode control of a 2-DOF direct-drive robot arm," *IEEE Trans. Syst., Man, Cybern. B, Cybern.*, vol. 38, no. 6, pp. 1561–1570, Dec. 2008.
[38] R. Oboe, F. Marcassa, and G. Maiocchi, "Hard disk drive with voltage-driven voice coil motor and model-based control," *IEEE Trans. Magn.*, vol. 41, no. 2, pp. 784–790, Feb. 2005.
[39] L. Encica, J. Makarovic, E. A. Lomonova, and A. J. A. Vandenput, "Space mapping optimization of a cylindrical voice coil actuator," *IEEE Trans. Ind. Appl.*, vol. 42, no. 6, pp. 1437–1444, Nov./Dec. 2006.
[40] J. Zheng, M. Fu, Y. Wang, and C. Du, "Nonlinear tracking control for a hard disk drive dual-stage actuator system," *IEEE/ASME Trans. Mechatronics*, vol. 13, no. 5, pp. 510–518, Oct. 2008.
[41] S.-K. Hung, E.-T. Hwu, M.-Y. Chen, and L.-C. Fu, "Dual-stage piezoelectric nano-positioner utilizing a range-extended optical fiber Fabry–Perot interferometer," *IEEE/ASME Trans. Mechatronics*, vol. 12, no. 3, pp. 291–298, Jun. 2007.
[42] F.-J. Lin and P.-H. Chou, "Adaptive control of two-axis motion control system using interval type-2 fuzzy neural network," *IEEE Trans. Ind. Electron.*, vol. 56, no. 1, pp. 178–193, Jan. 2009.
[43] X. Chen and T. Hisayama, "Erratum to 'adaptive sliding-mode position control for piezo-actuated stage'," *IEEE Trans. Ind. Electron.*, vol. 56, no. 2, p. 601, Feb. 2009.

Mei-Yung Chen received the B.S. degree from Tamkang University, Taipei, Taiwan, in 1992, the M.S. degree from Chung Yuan Christian University, Jhongli City, Taiwan, in 1994, and the Ph.D. degree from National Taiwan University, Taipei, in 2003.

He is currently an Associate Professor with the Department of Mechatronic Technology, National Taiwan Normal University, Taipei. His areas of research interest include magnetic levitation, positioning and tracking, mechatronics, and control theory and applications.

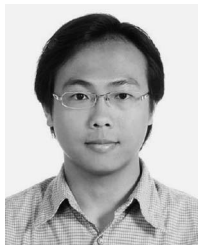

Hsuan-Han Huang received the B.S. and M.S. degrees from National Taiwan University, Taipei, Taiwan, in 2003 and 2005, respectively.

Since 2005, he has been a System Development Engineer with MediaTek Inc., Hsinchu, Taiwan, devoted in servo control system and firmware development in Blu-ray optical disk drives.

Shao-Kang Hung (M'03) received the B.S., M.S., and Ph.D. degrees from National Taiwan University, Taipei, Taiwan, in 1998, 2000, and 2007, respectively.

Since 2008, he has been on the faculty and is currently an Assistant Professor with the Department of Mechanical Engineering, National Chiao Tung University, Hsinchu, Taiwan. His research interests include optomechatronic systems, nanometer-scale instrumentation, precision motion control, and robotics.